Multi-Instrument Comparison of Top-of-Atmosphere Reflected Solar Radiation

Norman G. Loeb[1]
Center for Atmospheric Sciences, Hampton University, Hampton, Virginia[2]

Bruce A. Wielicki
NASA Langley Research Center, Hampton University, Hampton, Virginia

Wenying Su
Center for Atmospheric Sciences, Hampton University, Hampton, Virginia

Konstantin Loukachine
Science Applications International Corporation, Hampton, Virginia

Wenbo Sun
Center for Atmospheric Sciences, Hampton University, Hampton, Virginia

Takmeng Wong, Kory J. Priestley
NASA Langley Research Center, Hampton University, Hampton, Virginia

Grant Matthews
Analytical Services and Materials, Hampton, Virginia

Walter F. Miller
Science Applications International Corporation, Hampton, Virginia

R. Davies[3]
Jet Propulsion Laboratory, California Institute of Technology, Pasadena, California

Journal of Climate

Revised May, 2006

[1] *Corresponding Author Address*: Dr. Norman G. Loeb, Mail Stop 420, NASA Langley Research Center, Hampton, VA 23681-2199, U.S.A. (757) 864-5688 (office); (757) 864-7996 (fax);

Email: n.g.loeb@larc.nasa.gov

[2] Now at National Institute of Aerosospace, Hampton, VA
[3] Now at University of Auckland, New Zealand

Abstract

Observations from CERES, MODIS, MISR and SeaWiFS between 2000 and 2005 are analyzed in order to determine if these data are meeting climate accuracy goals recently established by the climate community. The focus is primarily on top-of-atmosphere (TOA) reflected solar radiances and radiative fluxes. Direct comparisons of nadir radiances from CERES, MODIS and MISR aboard the *Terra* satellite reveal that the year-to-year relative stability of measurements from these instruments is better than 1%, and shows no systematic change with time. By comparison, the climate requirement for the radiometric stability of visible radiometer measurements is 1% per decade. When tropical ocean monthly anomalies in shortwave (SW) TOA radiative fluxes from CERES on *Terra* are compared with anomalies in Photosynthetically Active Radiation (PAR) from SeaWiFS—an instrument whose stability is better than 0.07% during its first six years in orbit—the two are strongly anti-correlated. After scaling the SeaWiFS anomalies by a constant factor given by the slope of the regression line fit between CERES and SeaWiFS anomalies, the standard deviation in the difference between monthly anomalies from the two records is only 0.2 Wm^{-2}, and the difference in their trend lines is only 0.02±0.3 Wm^{-2} per decade, approximately within the 0.3 Wm^{-2} per decade stability requirement for climate accuracy. For both the tropics and globe, CERES *Terra* SW TOA fluxes show no trend between March 2000 and June 2005. Significant differences are found between SW TOA flux trends from CERES *Terra* and CERES *Aqua* between August 2002 and March 2005. This discrepancy is due to uncertainties in the adjustment factors used to account for degradation of the CERES *Aqua* optics during hemispheric scan mode operations. Comparisons of SW TOA flux between CERES *Terra* and the ISCCP FD RadFlux product show good agreement in monthly anomalies between January 2002 and December 2004, and poor agreement prior to this period. Commonly

used statistical tools applied to the CERES *Terra* data reveal that in order to detect a statistically significant trend of magnitude 0.3 Wm^{-2} per decade in global SW TOA flux, approximately 10 to 15 years of data are needed. This assumes that CERES *Terra* instrument calibration remains highly stable, long-term climate variability remains constant, and the *Terra* spacecraft has enough fuel to last 15 years.

1. Introduction

The exchange of radiant energy between the sun, Earth and space is fundamental to climate. The radiative energy balance that exists between solar radiation absorbed by Earth and thermal infrared radiation emitted back to space regulates the Earth's temperature and interacts directly with the components of the Earth-atmosphere system such as clouds, the surface, and the atmosphere. The Earth's outgoing fluxes have been observed to exhibit relatively large interannual variability during the past few decades: net radiation between 60°S-60°N has a peak-to-peak range of ±0.7 Wm^{-2} and a standard deviation of 0.43 Wm^{-2} (Wielicki et al., 2002; Wong et al., 2006). This variability is similar in magnitude to the variability in ocean heat storage measurements (Wong et al., 2006), and the anticipated change in anthropogenic radiative forcing over the next few decades (~0.6 Wm^{-2}) (IPCC, 2001). In order to achieve a more complete understanding of climate system variability, simultaneous independent observations of radiative fluxes and the Earth-Atmosphere components that influence the Earth radiation budget are needed. Unfortunately, the majority of long-term satellite data records available today were derived from satellite instruments whose calibration accuracy and stability is too crude to detect anticipated trends in anthropogenic forcing. To move forward, therefore, we must take a hard look at our more modern instruments and determine whether or not they are meeting the accuracy requirements needed to address climate change.

In order to proceed, it is first necessary to define quantitatively, variable-by-variable, what the climate requirements are. Recently, Ohring et al. (2005) reported on an ongoing effort in which scientists from several satellite groups gathered for a workshop whose goal was to "develop requirements and recommend directions for future improvements in satellite instrument characterization, calibration, intercalibration, and associated activities to enable measurements of global climate change that are valid beyond a reasonable doubt." The group produced a set of accuracy requirements for approximately 32 environmental variables derived from passive satellite instruments that make observations in spectral bands ranging from the ultraviolet to the microwave. Ohring et al. (2005) make a clear distinction between absolute accuracy and stability. Accuracy refers to the bias or systematic error of the data, while stability involves the extent to which the accuracy remains constant with time. Excellent absolute accuracy is vital for understanding climate processes and for model validation, whereas stability is needed for detecting long-term changes or trends in the data. As a result, stability requirements are generally more stringent than accuracy requirements. For example, Ohring et al. (2005) state that in order to meet climate requirements, imager visible radiances used to infer visible cloud optical depth need be accurate to 5% and stable to 1% per decade, and Earth Radiation Budget measurements need to be accurate to 1% and stable to 0.3% per decade (or equivalently, 0.3 Wm^{-2} per decade).

In this study, data from several state-of-the-art satellite instruments currently in orbit are analyzed and compared in order to determine whether or not data records emerging from these instruments appear to be meeting climate accuracy goals. The main emphasis here is on the stability of calibrated data records. The analysis is somewhat preliminary as it involves only up to 5 years of data from each instrument. Comparisons performed include direct radiance comparisons for three instruments aboard the *Terra* spacecraft, and comparisons of deseasonalized anomalies in large-scale monthly mean quantities such as top-of-atmosphere (TOA) reflected solar or shortwave (SW) flux. The main focus in this study is on SW radiation at the TOA. In the following, a detailed description of the observations from each instrument is provided, followed by comparisons of the relative radiometric stability and 5-year monthly anomalies from the different instruments. Based on the initial 5-year records, we employ commonly used statistical techniques to estimate the number of years of data needed to detect trends of comparable magnitude to the anticipated change in anthropogenic radiative forcing over the next few decades.

2. Observations

Table 1 provides a complete list of the datasets used in this study. The *Terra* satellite, launched in December 1999, is in a descending sun-synchronous near-polar orbit with an equator crossing time of 10:30 a.m. local time. Measurements from three of the five *Terra* instruments are considered. The Clouds and the Earth's Radiant Energy System (CERES) instrument (Wielicki et al. 1996) is a scanning thermistor bolometer that measures radiances in shortwave (0.3-5 µm), window (8-12 µm), and total (0.3 to 200 µm) channels at a spatial resolution of approximately ~20 km at nadir. CERES scans from limb-to-limb and provides global coverage each day. It can scan in three modes: cross-track, alongtrack, and rotating azimuth plane (RAP). Two CERES instruments, FM1 and FM2, are operating on *Terra*. The MODerate-resolution Imaging Spectroradiometer (MODIS) instrument (Salomonson et al., 1989; Barnes et al., 1998) measures narrowband radiances in 36 spectral bands from the visible to thermal infrared with a spatial resolution from 250 m to 1 km. It has a swath width of 2300 km and provides global coverage every 1-2 days. The Multi-angle Imaging SpectroRadiometer (MISR) instrument (Diner et al., 1998, 2002) provides information on bidirectional reflectance anisotropy and geometric parallax using nine alongtrack angles from nadir to 70º in four visible/near-infrared spectral bands with a spatial resolution of 275 m – 1.1 km. MISR has a 400 km swath width and provides global coverage in 2-9 days, depending on latitude. Two identical copies of CERES (FM3 and FM4) and one MODIS instrument also fly onboard the *Aqua* spacecraft, launched in

May 2002 in an ascending sun-synchronous near-polar orbit with an equatorial crossing time of 1:30 p.m. local time.

CERES, MODIS and MISR all use on-board calibration sources to monitor instrument calibration stability. To monitor changes in gain over the mission lifetime, each CERES instrument has on-board calibration sources for every channel. Concentric groove blackbodies are used for the window and total channels, and a stable tungsten lamp is used for the SW channel. While the SW channel signal from the internal calibration lamps has remained stable to the 0.2% level between 2000 and 2004 (Spence et al., 2004), comparison of independent observations from the two CERES *Terra* instruments indicates a decrease in reflected flux of 1.1% for FM1 and 1.6% for FM2 (Wielicki et al., 2005, Matthews et al., 2005). The effect was previously undetectable because the changes occurred in the blue-UV region, where tungsten lamp emission is very low. Direct comparisons of nadir radiance between CERES instruments in crosstrack and hemispherical scan modes suggest that the decrease in instrument response to SW radiance occurs when CERES operates in a hemispherical scan mode. The decrease is believed to be associated with contaminant deposition on the optics while the CERES telescope is pointed in the direction of spacecraft motion, which only occurs when CERES is in a hemispherical scan mode. Consequently, when the CERES instrument operates in the crostrack scan mode (i.e., perpendicular to the direction of motion) there should be no degradation in the response to SW radiance. A table of adjustment coefficients (so called “rev1” adjustment factors, Matthews et al, 2005) has been derived for user application to measurements made by CERES instruments on both *Terra* and *Aqua* satellites. Radiances and fluxes considered in this study have been adjusted using the “rev1” factors derived in Matthews et al (2005).

The MODIS design includes four onboard calibration modules: a solar diffuser, a solar diffuser stability monitor, a spectral radiometric calibration assembly, and a blackbody (Barnes et al., 1998). Two additional calibration techniques that MODIS uses are monthly views of the moon and deep space. A complete description of MODIS calibration performance during the first 4.5 years in orbit is available in Barnes et al. (2004b). The MISR instrument uses an on-board calibrator to provide updates to the instrument gain coefficients once every two months. The on-board calibrator consists of diffuse panels made of spectralon material and high quantum efficiency photodiodes, radiation-resistant photodiodes and a goniometer (Bruegge et al., 2002).

The CERES and MODIS data considered are from the CERES Single Scanner Footprint TOA/Surface Fluxes and Clouds (SSF) product (Geier et al., 2003, Loeb et al., 2003). The SSF product merges CERES parameters including time, position, viewing geometry, radiances and radiative fluxes with coincident information from MODIS, which is used to characterize the clear and cloudy portions of a CERES footprint. MODIS SSF parameters include radiances in 5 spectral bands for clear, cloudy and total areas, cloud property retrievals (Minnis et al., 1998; Minnis et al., 2003), and aerosol property retrievals from the MOD04 product (Remer et al., 2005), and a second aerosol retrieval algorithm applied to MODIS (Ignatov and Stowe, 2002). Radiances from only two MODIS bands—MODIS bands 1 (0.645 μm or 0.65 μm) and 2 (0.858 μm or 0.86 μm)—are considered in this study. Pixel-level radiances and cloud retrievals from MODIS are averaged over CERES footprints after weighting by the CERES point-spread function (PSF) (Smith 1994; Loeb et al. 2003). Also included in the SSF product are meteorological parameters (e.g., surface wind speed, skin temperature, precipitable water, etc.) from the Global Modeling and Assimilation Office (GMAO)'s Goddard Earth Observing System DAS (GEOS-DAS V4.0.3) product (Suarez, 2005).

The MISR data used in this study are from the SSFM Edition2B data product (Loeb et al., 2006) for selected days in each September between 2000 and 2004. The SSFM dataset consists of MISR Level 1B2 radiances that have been averaged over CERES footprints with the same algorithm used to average MODIS pixel-level data in the SSF product. Each CERES footprint contains average radiances from each of the nine MISR directions in all four spectral bands. The SSFM data product is only produced for days when CERES scans in the alongtrack mode (approximately twice per month).

The Sea-Viewing Wide-Field-of-View Sensor (SeaWiFS) (Hooker et al., 1992), launched in August 1997 onboard the SeaStar spacecraft, is an eight-band filter radiometer that measures radiances at 412, 443, 490, 510, 555, 670, 765, and 865 nm. SeaWiFS operates in a descending sun-synchronous polar orbit with a local noon equatorial crossing time. SeaWiFS uses routine lunar measurements (once per lunar month) to determine changes in its radiometric sensitivity (Barnes et al., 2004a). Based on the lunar calibration methodology, Eplee et al. (2004) show that SeaWiFS TOA radiances are stable to better than 0.07% during the first 2500 days (6 years and 10 months) since the first image was recorded. SeaWiFS daily (i.e., 24-hour averaged) Photosynthetically Active Radiation (PAR) retrievals between March 2000 and June 2005 are considered here. PAR is defined as the solar flux reaching the ocean surface in the 400-700 nm spectral range. It is derived from SeaWiFS TOA radiance measurements in the PAR spectral range (Patt et al., 2003) and is provided for all-sky conditions over ocean only.

SW radiative fluxes from the International Satellite Cloud Climatology Project (ISCCP) radiative flux profile data set (ISCCP-FD product) (Zhang et al., 2004) for March 2000 through December 2004 are also considered. To create the ISCCP-FD product, global satellite measurements are used to specify 3-hourly cloud, atmosphere and surface properties which are input to a radiative transfer model to compute radiative fluxes at the TOA, surface, and at several levels within the atmosphere. The ISCCP-FD product is an improved version of a previous ISCCP radiative flux product (ISCCP-FC) (Zhang et al., 1995). A comprehensive description of the input data used to produce the ISCCP data product is provided in Zhang et al. (2004). The satellite imaging radiometers used by ISCCP are designed primarily for weather applications for which accurate absolute calibrations were not emphasized (Rossow and Schiffer, 1999; Brest et al., 1997). Therefore, there are no on-board calibration sources or lunar measurements available to monitor the stability of the reflected solar channels from these satellites. Rather, ISCCP must provide the absolute calibrations through vicarious methods (Brest et al., 1997).

3. CERES-MISR-MODIS Radiometric Stability

Instrument calibration involves the use of both onboard calibration sources and vicarious calibration techniques to monitor and adjust the radiometric output of an instrument. If no calibration adjustments were made, most instruments would show significant levels of radiometric degradation (e.g., due to ultraviolet radiation exposure on the optics). The ability to compensate for instrument degradation through onboard sources and vicarious methods can only be done so accurately, however. Independent studies are thus needed to verify the stability of climate data records. This can involve examining time series of measurements from stable targets such as the moon, desert regions, deep convective clouds, etc., or intercomparisons amongst different calibrated instruments that observe the same region.

In the following, coincident measurements from CERES, MODIS and MISR are used to quantify the relative stability of data records from these instruments during the first five years of operation. As there is no one instrument flying that serves as the calibration stability "standard" in space, it is not possible based on these results alone to claim that one data record is more stable than another. Nevertheless, a direct comparison does serve to identify any obvious discrepancies and provides preliminary data to assess whether or not data records emerging from the instruments appear to be meeting climate accuracy goals.

3.1 MODIS Terra and CERES Terra Radiance Comparison

CERES and MODIS *Terra* near-nadir radiances are compared in order to examine if the two instruments have been stable relative to one another during their first five years of operation. The comparison is restricted to CERES FM1 cross-track SW radiances and MODIS radiances in the 0.65 μm (band 1) and 0.86 μm (band 2) bands from the CERES SSF product. To minimize the influence of scene dependent noise in the comparisons due to variations in the narrowband-to-broadband relationship between CERES and MODIS with scene type (Loeb et al., 2006), it is first necessary to average the CERES and MODIS measurements over relatively large spatial scales prior to determining their relative stability. Therefore, only CERES footprints over ocean between 30°S and 30°N with a viewing zenith angle smaller than 10° are considered. For each day of FM1 crosstrack data between March 2000 and June 2005, average tropical ocean CERES SW and MODIS narrowband radiances are calculated from 1° latitude-longitude equal-area average values. A linear regression fit is then applied to the daily average CERES and MODIS radiances in each month (with CERES radiance as the dependent variable). Results for May 2000 are shown in Fig. 1a and 1b for the 0.65 μm and 0.86 μm MODIS bands, respectively. In the 0.65 μm band, the coefficient of determination (r^2) is 0.997 and the coefficient of variation (CV, defined as the standard deviation of the residuals divided by the mean) is 0.3%. Similarly, in the 0.86 μm band, r^2 is 0.993 and CV is 0.4%.

Next, the regression equations in each month are used to produce estimates of the overall mean predicted CERES SW radiance from all available daily tropical mean MODIS radiances.

The predicted SW radiance based on regression coefficients in year *yr* and month *mn* is determined as follows:

$$\overline{I}_p^{sw}(yr,mn) = \sum_{j=1}^{n_d} \frac{I_{p,j}^{sw}(yr,mn)}{n_d} = \sum_{j=1}^{n_d} \frac{a_o(yr,mn) + a_1(yr,mn) I_j}{n_d} \qquad (1)$$

where a_o and a_1 are the intercept and slope of the regression, I_j is the daily tropical mean MODIS radiance on day *j*, and n_d is the number of daily tropical mean MODIS radiances used (here n_d=1933). The year-to-year relative calibration stability of CERES and MODIS is determined by comparing predicted mean CERES radiances from regression coefficients in each year with those in 2000 as follows:

$$\Delta(yr) = \frac{\frac{1}{n_m} \sum_{mn} \overline{\delta}(yr,mn) \pm t_{n_m-1}\, s_{\overline{\delta}}(yr)}{\frac{1}{n_m} \sum_{mn} \overline{I}_p^{sw}(2000,mn)} \qquad (2)$$

where,

$$\overline{\delta}(yr,mn) = \overline{I}_p^{sw}(yr,mn) - \overline{I}_p^{sw}(2000,mn) \qquad (3)$$

$$s_{\overline{\delta}}(yr) = \sqrt{\frac{\sum_{mn} (\overline{\delta}(yr,mn) - \overline{\overline{\delta}}(yr))^2}{n_m - 1}} \qquad (4)$$

$$\overline{\overline{\delta}}(yr) = \sum_{mn} \frac{\overline{\delta}(yr,mn)}{n_m} \qquad (5)$$

t_{n_m-1} is derived from the Student-t distribution for n_m-1 degrees of freedom at the 95% significance level, and n_m is the number of months in which FM1 cross-track data are available in both year *yr* and in 2000. If both CERES and MODIS calibration remained perfectly stable during the first five years of operation, or if the calibration of both instruments drifted by the same amount each year, then Δ would be zero in each of the five years.

Fig. 2 shows the year-to-year relative calibration stability of CERES and MODIS as defined in Eq. (2) between 2001 and 2005 for the 0.65 μm (red) and 0.86 μm (near-infrared) bands. In both bands, the relative calibration of CERES and MODIS has remained stable to better than 1%. Between 2001 and 2003, Δ is negative in both channels, while it is close to 0% for 2004-2005. A negative value of Δ can occur if the change in MODIS calibration is larger than the change in CERES calibration, and the MODIS calibration change causes radiances in a given year to be larger than those in 2000. A negative Δ can also occur if the change in CERES calibration is larger than the change in MODIS calibration, and the CERES calibration change causes radiances in a given year to be smaller than those in 2000. Both of these possibilities imply a decrease in the slopes of regression line fits to data in a given year compared to 2000. Note that from these results alone, it is not possible to tell which of the above two possibilities has occurred.

Because the CERES measurement is a broadband radiance while the MODIS measurement is a narrowband radiance, a nonzero Δ can also occur if there is a shift in the relative spectral composition of the tropics with time. For example, any systematic changes in cloud and aerosol properties or their frequency-of-occurrence (e.g., fewer clouds, lower clouds) will likely have a different effect on the broadband measurement than on the narrowband measurement. If present, such changes could be misinterpreted as relative calibration changes in this analysis.

3.2 MISR and MODIS *Terra* Radiance Comparisons

In order to assess the relative stability of MISR and MODIS, MISR nadir radiances in the SSFM Edition2B data product (Loeb et al., 2006) are directly compared with MODIS nadir radiances in the SSF data product. Radiances from both instruments have been averaged over the same CERES footprints and weighted by the CERES PSF. Because MISR and MODIS are narrowband instruments with similar spectral bands, their relative calibration stability can be determined with fewer days than what is needed to compare CERES and MODIS. In addition, any changes in the relative spectral composition of the tropics with time will have a much smaller influence in the MISR/MODIS comparison than the CERES/MODIS comparison. Two September days per year for every year between 2000 and 2004 (ten days total) are used to compare MISR and MODIS. Figs. 3a and 3b show scatter plots of MISR and MODIS radiances from September 12, 2000, in the red and near-infrared bands, respectively. Each point corresponds to an individual instantaneous footprint average radiance. In the red band (Fig. 3a), the correlation is excellent, with r^2=0.999 and CV =3.2 %. In the near-infrared band, the MODIS saturates for very bright scenes as is clearly evident from Fig. 3b. To avoid introducing errors due to saturation, only MODIS near-infrared radiances smaller than 200 Wm^{-2} sr^{-1} μm^{-1} are considered. With this criterion, the r^2 for MISR and MODIS near-infrared radiances is 0.998 and CV is 3.6%.

Linear regression fits are derived from MISR and MODIS radiances from each of the ten available September days between 2000 and 2004. The regression coefficients from each day are then applied to produce ten sets of predicted red and near-infrared MISR radiances averaged over the tropical oceans (c.f. Eq. (1)). The relative stability of MISR and MODIS is determined by comparing predicted mean MISR radiances in a given year with the predicted radiances in 2000.

Fig. 4 shows the year-to-year relative calibration stability of MISR and MODIS as defined in Eq. (2) between 2001 and 2004 for the 0.65 μm (red) and 0.86 μm (near-infrared) bands. The relative calibration of MISR and MODIS has remained stable to better than 1% in the red band and 0.5% in the near-infrared band. Interestingly, in all comparisons Δ is negative. As noted earlier, Δ was also generally negative for the same period in the CERES and MODIS comparisons (Fig. 2). Thus, it would appear that either MODIS calibration changes caused MODIS radiances to increase relative to 2000 or changes in both CERES and MISR calibration caused those radiances to decrease relative to 2000. Again, from these data alone, it is only possible to identify relative calibration changes between the instruments, not the actual calibration change of the individual instruments.

A relative stability of 1% or better between CERES, MODIS and MISR is encouraging. As noted earlier, Ohring et al. (2005) state that in order to meet climate requirements, imager visible radiances used to infer trends in visible cloud optical depth need be stable to 1% per decade, while Earth Radiation Budget measurements need to be stable to 0.3%. As the differences between CERES, MODIS and MISR in Figs. 2 and 4 show no systematic temporal dependence, the results are not inconsistent with the requirements in Orhing et al. (2005). Clearly, a longer time series is needed to verify this.

4. Deseasonalized Anomalies

In order to compare climate data records from different instruments, it is convenient to compare anomalies in the monthly time series after removing the seasonal cycle in the data. A deseasonalized monthly anomaly is determined by differencing the average in a given month from the average of all years of the same month. Deseasonalized anomalies of a variable *X* are determined as follows:

$$\Delta X(yr, mn) = X(yr, mn) - \bar{X}(mn) \qquad (6)$$

where $X(yr, mn)$ is the monthly mean of X in year "yr" and month "mn", and $\bar{X}(mn)$ is the average of X from all years of month "mn".

4.1 CERES *Terra* SW TOA Flux and SeaWiFS PAR

Fig. 5a shows deseasonalized monthly anomalies in SeaWiFS PAR and CERES FM1 SW TOA flux over ocean for 30°S-30°N from March 2000 through June 2005. Since PAR is an estimate of the 400-700 nm radiation reaching the surface and CERES SW flux is an estimate of the reflected solar flux at the TOA, the two are anti-correlated. The CERES SW TOA flux anomalies remain relatively constant throughout the period except for a brief decrease during the second half of 2003, followed by rapid fluctuations in early 2004. The maximum SW TOA flux anomaly in March 2004 coincides with the minimum anomaly in PAR. The March 2004 anomaly is approximately 4 times larger than the standard deviation in monthly anomalies for the entire period.

When SW TOA flux and PAR anomalies are plotted against one another, the r^2 value is 0.93 and the slope of the regression line is –6.60 Wm^{-2} per E m^{-2} day^{-1}. Fig. 5b shows the same results as in Fig. 5a after scaling the PAR monthly anomalies by the slope of the regression line. The correspondence between the CERES and SeaWiFS anomalies is quite remarkable. The standard deviation in the monthly anomalies for both data records is approximately 0.8 Wm^{-2} and the standard deviation in the difference between CERES and SeaWiFS monthly anomalies is 0.21Wm^{-2} (Table 2), a factor of 4 smaller than the month-to-month variability. Neither CERES *Terra* nor SeaWiFS indicate any significant systematic change during the period considered

(Table 3). The slope in the SeaWiFS anomalies is 0.41±1.2 Wm^{-2} per decade, compared to 0.43±1.5 Wm^{-2} per decade for CERES. The two are consistent to 0.02±0.3 Wm^{-2} per decade, where ±0.3 Wm^{-2} per decade corresponds to the 95% confidence interval. This difference comes very close to falling within the 0.3 Wm^{-2} per decade stability requirement in Ohring et al. (2005). Part of the difference between SeaWiFS and CERES may occur because SeaWiFS PAR is a narrowband (0.4 to 0.7 μm) quantity while CERES SW TOA flux is broadband. Therefore, trends from these two data sets will generally be closer for spectrally flat albedo targets (e.g., clouds) compared to targets such as snow and ice, land, and aerosol.

Table 4 compares CERES and SeaWiFS anomalies for four tropical ocean regions. In two of these regions (southwest tropics and northwest tropics), the CERES and SeaWiFS anomaly trends are significantly different. The most likely reason for the different trends is regional changes in cloud and aerosol properties. Such changes can alter the narrow-to-broadband relationship between SW flux and PAR with time, thereby leading to different anomaly trends.

The broadband-narrowband differences between the CERES and SeaWiFS measurements also influences the slope of the regression line between SW TOA flux and PAR anomalies. While the –6.60 Wm^{-2} per E m^{-2} day^{-1} regression line slope obtained in this analysis is consistent with radiative transfer calculations for typical cloud and aerosol conditions (not shown), the slope does show some sensitivity to regional variations in cloud and aerosol properties. Fig. 6 shows the slope of the SeaWiFS PAR—CERES SW flux anomaly regression line for the tropical ocean regions listed in Table 4. For these relatively large-scale oceanic regions, the slope varies by approximately 15%. Larger differences are expected over land and snow.

Interestingly, the slope in the CERES *Terra* SW TOA flux anomalies for the entire tropics (ocean and land) is of the opposite sign to that for ocean only (Table 3). For the entire tropics, the slope is -0.26 ± 1.3 Wm^{-2} per decade compared to 0.43 ± 1.5 Wm^{-2} per decade for ocean only. This difference is associated with SW TOA flux changes over land. Fig. 7a shows the land SW TOA flux anomalies averaged over the tropics together with the multivariate ENSO index (MEI, Wolter and Timlin, 1993, 1998). The land SW TOA flux anomalies decrease by -0.69 ± 0.5 Wm^{-2} per decade and are anti-correlated with the MEI, as indicated in Fig. 7b (the slope of the line in Fig. 7b is -0.33 ± 0.14 Wm^{-2}). These results suggest that SW TOA fluxes tend to be smaller over land during El Niño events and larger during periods of La Niña. In contrast, a similar scatterplot of tropical ocean SW TOA flux anomalies versus MEI failed to show a significant relationship (not shown). For the entire globe, the decrease in reflectance is more pronounced, at -0.59 ± 0.9 Wm^{-2} per decade.

4.2 CERES Terra and CERES Aqua SW TOA Flux

A direct comparison of SW TOA flux anomalies from CERES *Terra* FM1 and CERES *Aqua* FM4 for August 2002 through March 2005 is provided in Figs. 8a and 8b. During the first 12 months (up to July 2003), CERES *Aqua* SW TOA flux anomalies exceed those of CERES *Terra*, while the opposite is true during the last 13 months from March 2004 through March 2005. The CERES *Aqua* TOA fluxes systematically decrease by 3.5 Wm^{-2} per decade in the tropics and 2.9 Wm^{-2} per decade for the globe (Table 3), while CERES *Terra* anomalies remain relatively constant (< 1 Wm^{-2} per decade). Both records indicate that the variability in all-sky SW TOA fluxes in the tropics exceeds that for the entire globe by approximately 70% (Table 2). While the standard deviation in the CERES *Aqua* and *Terra* monthly anomalies is consistent to

0.4 Wm^{-2}, the correlation between the two records is quite low—r^2 is only 0.75 for the tropics and 0.47 for the globe.

As is indicated in Table 3, the difference between the slope of the regression lines in Figs. 8a and 8b are significant at the 95% level. The discrepancy is believed to be due to uncertainties in the adjustment factors used to account for degradation of the CERES FM4 SW channel optics during hemispheric scan mode operations. While such adjustments are made for both CERES FM1 and FM4, the methodology used to derive the adjustment factors was found to work far better for CERES Terra than for CERES Aqua, suggesting that either FM4 optics continued to degrade in crosstrack mode or the FM4 onboard lamb got brighter during the mission (as was observed with the CERES instrument on the Tropical Rainfall Measuring Mission satellite).

4.3 CERES Terra and ISCCP FD RadFlux SW TOA Flux

Figs. 9a and 9b compare SW TOA flux anomalies from CERES *Terra* and the ISCCP FD RadFlux data product (Zhang et al., 2004) for March 2000 through December 2004. ISCCP FD RadFlux anomalies show approximately 40% more variability than CERES *Terra* in the tropics, and are almost twice as variable as CERES *Terra* globally (Table 2). The correlation between the two data records is also quite low, with r^2 values of 0.43 in the tropics and 0.19 globally. Interestingly, the month-to-month agreement between the two data records is markedly better from January 2002 onwards compared to the first 22 months. ISCCP radiative flux anomalies prior to January 2002 are far more variable than both CERES *Terra* anomalies and ISCCP anomalies after January 2002.

In the tropics, both ISCCP and CERES *Terra* SW TOA flux anomalies show modest changes (Table 3). ISCCP anomalies increase by 0.75±2.3 Wm^{-2} per decade while CERES *Terra* anomalies decrease by 0.64±1.5 Wm^{-2} per decade. Globally, the ISCCP SW TOA flux anomalies show a much larger increase of 1.8 ± 2 Wm^{-2} per decade, while CERES *Terra* anomalies decrease by 0.76 ± 1 Wm^{-2} per decade. While neither of these changes is significant at the 95% level, the difference in the slopes is significant (2.5±1.7 Wm^{-2} per decade). We note that despite these differences, the ISCCP results fall well within the 3-5% relative calibration uncertainty estimated by Brest et al. (1997).

4.4 Trend Analysis

The recent advances in technology and onboard calibration have led to significant improvements in the radiometric stability of current state-of-the-art satellite instruments such as those considered in this study. Older instruments such as the Advanced Very High Resolution (AVHRR) series of sensors which had no onboard calibration in the visible channels typically degraded by 1-3% per year (Brest et al., 1997; Tahnk et al., 2001). If the newer instruments continue to collect data until the spacecraft they fly on exhaust all of the available fuel (nominally 15 years for *Terra* and *Aqua*), how small a trend can we expect to be able to observe assuming instrument calibration remains stable? The question is critical given that greenhouse gas radiative forcing is approximately 0.6 Wm^{-2} per decade (IPCC, 2001), and a 50% change in climate sensitivity due to cloud feedback would arise from a net cloud radiative effect change of only 0.3 Wm^{-2} per decade: either stabilizing or de-stabilizing. Narrowing climate prediction uncertainty to a factor of 2 thus requires verification of cloud feedback at the level of 0.3 Wm^{-2} change per decade. According to Weatherhead et al. (1998), trend detectability depends upon three major factors: (i) the size of the trend to be detected; (ii) the unexplained variability in the data (e.g., natural climate variability); and (iii) the autocorrelation of the noise in the data. Following techniques commonly used to assess trends in environmental data, Weatherhead et al.

(2000) derive the following expression to determine the number of years (n^*) required to detect a trend of magnitude ω_o, with at least 1-β probability:

$$n^* \approx \left[\frac{(2+z_\beta)}{|\omega_o|} \sigma_N \sqrt{\frac{1+\phi}{1-\phi}} \right]^{2/3} \tag{7}$$

where σ_N is the month-to-month variability in the data, ϕ is the autocorrelation in the month-to-month data with a lag of one month, and $-z_\beta$ is the lower β-percentile of the standard normal distribution, such that $P(Z < -z_\beta) = \beta$. Here Z is the standard normal random variate of the estimated trend. From Weatherhead et al. (2000), setting z_β=0 in Eq. (7) provides the number of years needed to detect a trend of magnitude ω_o at the 95% significance level with a probability of 50%. Similarly, using z_β=1.3 in Eq. (7) provides the number of years needed to detect a trend of magnitude ω_o at the 95% significance level with a probability of 90%.

Figs. 10a and 10b show the number of years needed to detect trends in all-sky tropical and global CERES *Terra* SW TOA flux, respectively, with probabilities of 50% and 90%. We assume that the CERES *Terra* instrument calibration remains stable throughout the record and ignore any unforeseen events (e.g., major volcanic eruptions) that may significantly alter the variability and autocorrelation in the data collected after the initial first 5 years. In order to detect a trend in global SW TOA flux that is 50% of the 0.6 Wm^{-2} anticipated change in anthropogenic radiative forcing over the next few decades, approximately 10 to 15 years of data are needed (the lower bound occurs with 50% probability, while the upper bound occurs with 90% probability). Because the variability is greater in the tropics, the number of years to detect a 0.3 Wm^{-2} per decade trend is also greater, at 14 to 20 years.

5. Discussion

The results presented in this study are in stark contrast to those of Pallé et al. (2004, 2005) who claim to have observed a 6 Wm^{-2} increase in annual mean reflected solar radiation between 2000 and 2003 based on Earthshine measurements. As noted by Wielicki et al. (2005), an increase of 6 Wm^{-2} is a factor 2.4 times larger than the anomaly caused by the Mount Pinatubo eruption. Since there is no evidence of a significant event (such as a volcanic eruption) between 2000 and 2003 large enough to produce such a dramatic change in the Earth's reflectance, it is unclear why the Earthshine anomaly is so large. When the global monthly anomalies in CERES *Terra* SW TOA flux in Fig. 9b are averaged annually, the difference between the minimum and maximum yearly anomalies is 0.6 Wm^{-2}, an order-of-magnitude smaller than the change found in the Earthshine data. Given the remarkable consistency shown here between data records from CERES, MODIS, MISR, SeaWiFS and ISCCP, none of these additional data records support a 6 Wm^{-2} change between 2000 and 2003.

Trends of even a few tenths of a percent in global reflected SW flux can have a significant effect on climate sensitivity if uncompensated for by greenhouse cloud effects (e.g., low cloud changes). For example, if the anthropogenic forcing of climate is 0.6 Wm^{-2} per decade (IPCC, 2001), a trend of -0.6 Wm^{-2} per decade in global reflected SW flux would be sufficient to double global temperature climate sensitivity; a trend of +0.3 Wm^{-2} per decade would reduce climate sensitivity in half. Clearly, some of the SW flux trends due to clouds will likely be compensated by greenhouse thermal infrared effects of clouds. The magnitude of the compensation will depend upon whether the changes occur in low or high clouds: if the changes are dominated by low cloud changes, then compensation by greenhouse thermal infrared effects of clouds will be small, conversely, if the changes occur in high clouds, significantly stronger compensation is likely.

6. Summary and Conclusions

Data from several state-of-the-art satellite instruments currently in orbit were analyzed and compared in order to determine if data records emerging from these instruments are meeting climate accuracy goals established by the climate community (Ohring et al., 2005). The relative stability of radiance measurements from CERES, MODIS and MISR aboard the *Terra* spacecraft during the first 5 years of operation is determined from a regression analysis of highly collocated and coincident nadir radiances from the three instruments. To determine the relative stability of CERES and MODIS radiances, CERES FM1 cross-track SW radiances and MODIS radiances in the 0.65 μm (band 1) and 0.86 μm (band 2) bands from the CERES SSF product are used. Each day, average tropical ocean CERES SW and MODIS narrowband radiances are calculated from 1° latitude-longitude equal-area average values. A linear regression fit is applied to the daily tropical averages each month CERES FM1 operates in crosstrack mode during the 5-year period. The regression equations in each month and year are used to produce a time-series of predicted monthly tropical mean CERES SW radiances from the MODIS radiances in each band. The year-to-year relative calibration stability of CERES and MODIS is determined by comparing predicted mean CERES radiances from regression coefficients in each month and year with the predicted mean radiance in the year 2000 for the corresponding month. In both bands, the relative calibration of CERES and MODIS has remained stable to better than 1%. Between 2001 and 2003, either MODIS radiances increased slightly relative to CERES or CERES radiances decreased slightly relative to MODIS.

To compare MODIS and MISR nadir radiances, a new merged CERES and MISR dataset (called the SSFM data product) that spatially averages MISR radiances over CERES footprints in the same manner as MODIS radiances are averaged on the CERES SSF product is used. Coincident MISR and MODIS data from ten September days between 2000 and 2004 are considered. For each day, a regression line is fit to instantaneous MISR and MODIS data over the tropical oceans. The relative stability of MISR and MODIS is determined by comparing predicted mean MISR radiances in a given year with the predicted radiances in 2000. We find that the relative calibration of MISR and MODIS has remained stable to better than 1% in the red band and 0.5% in the near-infrared band. Also, the relative differences between MISR and MODIS are quite similar to those between CERES and MODIS for the same period. Between 2001 and 2004, either MODIS radiances increased relative to both CERES and MISR, or CERES and MISR radiances both decreased relative to MODIS. From these data alone, it is only possible to identify relative calibration changes between the instruments, not the actual calibration change of the individual instruments. Nevertheless, the results are encouraging. The relative calibration stability between CERES, MODIS and MISR show no obvious systematic temporal dependence. Therefore, if the instruments continue to maintain their current levels of calibration stability throughout the mission, results in this study suggest that climate data records from these instruments are likely meet the climate accuracy goals outlined in Ohring et al. (2005).

One of the most stable Earth-viewing satellite instruments in orbit is the SeaWiFS instrument, which has been shown to be stable to better than 0.07% during the six years in orbit. When deseasonalized anomalies in tropical ocean mean CERES SW TOA flux are compared with SeaWiFS PAR retrievals, the two are strongly anti-correlated. After scaling the SeaWiFS PAR anomalies by the slope of a regression line fit between CERES SW TOA flux and SeaWiFS

PAR anomalies in order to place the two data records on the same radiometric scale, the monthly anomalies from the two datasets are consistent to 0.2 Wm^{-2}, and the difference between their linear trends is 0.02±0.3 Wm^{-2} per decade (with 95% confidence). The agreement is close to the 0.3 Wm^{-2} per decade stability requirement outlined in Ohring et al. (2005). In contrast to recent Earthshine results of Pallé et al. (2004, 2005), neither CERES *Terra* nor SeaWiFS indicate any significant systematic change in SW radiative flux during the period considered.

Despite the excellent agreement between CERES and SeaWiFS anomaly trends over the entire tropics, significant differences were observed when anomalies over smaller areas, such as the southwest and northwest tropics, were compared. The most likely reason for the different regional trends is changes in cloud and aerosol properties. Such changes can alter the narrow-to-broadband relationship between SW flux and PAR with time, leading to different anomaly trends. Therefore, in order to obtain an accurate quantitative account of long-term changes in both regional and global TOA radiation, stable measurements of the entire SW spectral region are necessary.

While the tropical ocean mean CERES *Terra* and SeaWiFS data records show excellent agreement, the same is not true of CERES *Terra* and CERES *Aqua*. For the period of August 2002 through March 2005, CERES *Aqua* TOA fluxes systematically decrease by 3.5 Wm^{-2} per decade in the tropics and 2.9 Wm^{-2} per decade for the globe, while CERES *Terra* anomalies remain smaller than 1 Wm^{-2} per decade. The difference between the slopes of the regression lines is significant at the 95% level. This discrepancy is believed to be due to the adjustment factors used to account for ultraviolet radiation exposure of the CERES *Aqua* optics during hemispheric scan mode operations. Efforts are underway to improve these corrections.

The CERES *Terra* SW TOA flux anomalies were also compared with those from the ISCCP FD RadFlux data product for March 2000 through December 2004. In general, the correlation between the two data records is also quite low, with r^2 values of 0.43 in the tropics and 0.19 globally. Global trend differences between these records as determined from the difference between the slopes of regression line fits to the two data records is significant (2.5±1.7 Wm^{-2} per decade). We note that most of the discrepancy is mainly due to differences in monthly anomalies between March 2000 and January 2002. During this period, ISCCP radiative flux anomalies are highly variable compared to those of CERES *Terra* for the same period and ISCCP anomalies after January 2002.

Given that greenhouse gas radiative forcing is approximately 0.6 Wm^{-2} per decade (IPCC, 2001), and a 50% change in climate sensitivity due to cloud feedback would arise from a net cloud radiative effect change of only 0.3 Wm^{-2} per decade, the question arises as to how long a data record would be needed to detect a trend of this magnitude in observations of global SW TOA flux, given the natural variability and autocorrelation in the data. Common statistical techniques were used to address this question under the assumption that CERES *Terra* calibration remains highly stable and long-term climate variability remains constant during the *Terra* record. Results show that in order to detect a 0.3 Wm^{-2} per decade trend in global SW TOA flux, approximately 10 to 15 years of data are needed.

Acknowledgements

This work was supported by NASA Clouds and the Earth's Radiant Energy System Grant NNL04AA26G and NASA Grant NNG04GM13G. The research of R. Davies was conducted at the Jet Propulsion Laboratory, California Institute of Technology, under contract with NASA. The CERES SSF and MISR L1B2 data were obtained from the NASA Langley Research Center

Atmospheric Sciences Data Center. The ISCCP-FD data were provided by Y-C. Zhang. The authors would like to thank E. C. Weatherhead for helpful comments regarding the statistical analysis of the data.

References

Barnes, R. A., R. E. Eplee, Jr., F. S. Patt, H. H. Kieffer, T. C. Stone, G. Meister, J. J. Butler, and C. R. McClain, 2004a: Comparison of SeaWiFS measurements of the moon with the U.S. Geological Survey lunar model, *Appl. Optics*, **43**, 5838- 5854.

Barnes, R. A., R. E., Eplee, Jr., G. M. Schmidt, F. S. Patt, and C. R. McClain, 2001: Calibration of SeaWiFS. I. Direct techniques, *Appl. Opt*., **40**, 6683-6700.

Barnes, W. L., T.S. Pagano, and V.V. Salomonson, 1998: Prelaunch characteristics of the Moderate Resolution Imaging Spectroradiometer (MODIS) on EOS-AM1, *IEEE Trans. Geosci. Remote Sens.*, **36**, 1088–1100.

Barnes, W. L., X. Xiaoxiong, and V. V. Salomonson, 2004b: MODIS instrument status and operational activities, in Earth Observing Systems, IX, edited by W. L. Barnes and J. J. Butler, *Proc. of SPIE*, **5542**, doi: 10.1117/12.558185, pp. 14-23.

Brest, C. L., W. B. Rossow, and M. D. Roiter, 1997: Update of radiance calibrations for ISCCP, *J. Atmos. Oceanic Technol*., **14**, 1091–1109.

Bruegge, C. J., N. L. Chrien, R. R. Ando, D. J. Diner, W. A. Abdou, M. C. Helmlinger, S. H. Pilorz, and K. J. Thome, 2002: Early validation of the Multi-angle Imaging SpectroRadiometer (MISR) radiometric scale, *IEE Trans. Geosci. Remote Sensing*, **40**, 1477-1492.

Diner, D. J., J. C. Beckert, T. H. Reilly, C. J. Bruegge, J. E. Conel, R. Kahn, J. V. Martonchik, T. P. Ackerman, R. Davies, S. A. Gerstl, H. R. Gordon, J. P. Muller, R. B. Myneni, P. J. Sellers, B. Pinty, and M. M. Verstraete, 1998: Multiangle Imaging SprectroRadiometer (MISR) description and experiment overview, *IEEE Transactions on Geoscience and Remote Sensing*, **36,** 1072-1087.

Diner, D. J., J.C. Beckert, G. W. Bothwell, and J. I. Rodriguez, 2002: Performance of the MISR instrument during its first 20 months in Earth orbit, *IEEE Trans. Geosci. Remote Sensing.* **40**, 1449-1466.

Eplee, R.E., Jr., R. A. Barnes, F. S. Patta, G. Meisterb, and. C. R. McClain, 2004: SeaWiFS Lunar Calibration Methodology after Six Years on Orbit, in Earth Observing Systems IX, W.L. Barnes, J. J. Butler, ed., *Proc. SPIE*, 5542, doi: 10.1117/12.556408, p. 1-13.

Geier, E.B., R. N. Green, D. P. Kratz, P. Minnis, W. F. Miller, S. K. Nolan, and C. B. Franklin, 2003: Single satellite footprint TOA/surface fluxes and clouds (SSF) collection document. [available on-line from http://asd-www.larc.nasa.gov/CERES ASDceres.html.]

Hooker, S. B., W. E. Esaias, G. C. Feldman, W. W. Gregg, and C. R. McClain, 1992: An overview of SeaWiFS and ocean color, SeaWiFS Tech. Rep. Ser., Vol. 1, NASA Tech memo, 104566.

Ignatov, A. and L. L. Stowe, 2002: Aerosol retrievals from individual AVHRR channels: I. Retrieval algorithm and transition from Dave to 6S radiative transfer model. *J. Atmos. Sci.*, **59**, 313-334.

Intergovernmental Panel on Climate Change (IPCC), 2001: *Climate Change 2001: The Scientific Basis, Contribution of Working Group I to the Third Assessment Report of the Intergovernmental Panel on Climate Change*, edited by J. T. Houghton et al., Cambridge Univ. Press, New York, 2001.

Loeb, N. G., S. Kato, K. Loukachine, and N. M. Smith, 2005: Angular distribution models for top-of-atmosphere radiative flux estimation from the Clouds and the Earth's Radiant Energy

System instrument on the *Terra* Satellite. Part I: Methodology, *J. Ocean and Atmos. Tech.*, 22, 338-351.

Loeb, N. G., N. M. Smith, S. Kato, W. F. Miller, S. K. Gupta, P. Minnis, and B. A. Wielicki, 2003: Angular distribution models for top-of-atmosphere radiative flux estimation from the Clouds and the Earth's Radiant Energy System instrument on the Tropical Rainfall Measuring Mission Satellite. Part I: Methodology, *J. Appl. Meteor*., 42, 240-265.

Loeb, N. G., W. Sun, W. F. Miller, K. Loukachine, and R. Davies, 2006: Fusion of CERES, MISR and MODIS measurements for top-of-atmosphere radiative flux validation, *J. Geophys. Res*., (submitted).

Matthews, G., K. J. Priestley, P. Spence, D. Cooper, and D. Walikainen, 2005: Compensation for spectral darkening of short wave optics occurring on the Cloud's and the Earth's Radiant Energy System, in Earth Observing Systems X, edited by James J. Butler, *Proceedings of SPIE* , **5882**, doi: 10.1117/12.618972.

Minnis, P., D. P. Garber, D. F. Young, R. F. Arduini, and Y. Tokano (1998), Parameterizations of reflectance and effective emittance for satellite remote sensing of cloud properties, *J. Atmos. Sci*., *55*, 3313-3339.

Minnis, P., D. F. Young, S. Sun-Mack, P. W. Heck, D. R. Doelling, and Q. Trepte, 2003: CERES Cloud Property Retrievals from Imagers on TRMM, *Terra*, and *Aqua*, *Proc. SPIE 10th International Symposium on Remote Sensing: Conference on Remote Sensing of Clouds and the Atmosphere VII*, Barcelona, Spain, September 8-12, 37-48.

Ohring, G., B. A. Wielicki, R. Spencer, B. Emery, and R. Datla, 2005: Satellite instrument calibration for measuring global climate change: Report of a Workshop, *Bull. Amer. Met. Soc.*, **86**, 1303-1313.

Pallé, E., P. R. Goode, P. Montañés-Rodriguez, and S. E. Koonin, 2004: Changes in the Earth's reflectance over the past two decades, *Science*, **304**, 1299–1301, doi:10.1126/science.1094070.

Pallé, E., P. Montañés-Rodriguez, P. R. Goode, S. E. Koonin, M. Wild, and S. Casadio, 2005: A multi-data comparison of shortwave climate forcing changes, Geophys. Res. Letters, **32**, L21702, doi:10.1029/2005GL023847.

Patt, F. S., R. A. Barnes, R. E. Eplee, Jr., B. A. Franz, W. D. Robinson, G. C. Feldman, S. W. Bailey, J. Gales, P. J. Werdell, M. Wang, R. Frouin, R. P. Stumpf, R. A. Arnone, R. W. Gould, Jr., P. M. Martinolich, V. Ransibrahmanakul, J. E. O'Reilly, and J. A. Yoder, 2003: Algorithm updates for the fourth SeaWiFS data reprocessing, NASA Tech. Memo. 2003--206892, **22**, S.B. Hooker and E.R. Firestone, Eds., NASA Goddard Space Flight Center, Greenbelt, Maryland, 74 pp. [Available online from: http://oceancolor.gsfc.nasa.gov/cgi/postlaunch_tech_memo.pl?22].

Remer, L. A., Y. J. Kaufman, D. Tanré, S. Mattoo, D. A. Chu, J. V. Martins, R-R. Li, C. Ichoku, R. C. Levy, R. G. Kleidman, T. F. Eck, E. Vermote, and B. N. Holben (2005), The MODIS Aerosol Algorithm, Products and Validation, *J. Atmos. Sci., 62*, 947-973.

Rossow, W. B., and R. A. Schiffer, 1999: Advances in understanding clouds from ISCCP, *Bull. Amer. Soc.*, **80**, 2261-2287.

Salomonson, V. V., W. L. Barnes, P. W. Maymon, H. E. Montgomery, and H. Ostrow (1989), MODIS: Advanced facility instrument for studies of the earth as a system, *IEEE Transactions on Geoscience and Remote Sensing, 27(2)*, 145-153.

Smith, G. L., 1994: Effects of time response on the point spread function of a scanning radiometer. *Appl. Opt.*, **33**, 7031-7037.

Spence, P., K. J. Priestley, E. Kizer, S. Thomas, D. Cooper, and D. Walikainen, 2004: Correction of drifts in the measurements of the clouds and the earth's radiant energy system scanning thermistor bolometer instruments on the *Terra* and *Aqua* satellites, in Earth Observing Systems IX, W. L. Barnes and J. J. Butler, eds., *Proc. SPIE* **5542**, pp. 53–64.

Suarez, M. J. (2005), Technical report series on global modeling and data assimilation, Vol. 26: Documentation and validation of the Goddard Earth Observing System (GEOS) data assimilation system—Version 4, NASA/TM—2005—104606, Vol. 26, 181 pp., Washington, DC.

Tahnk, W. R., and J. A. Coakley, Jr., 2001: Improved calibration coefficients for NOAA-14 AVHRR visible and near-infrared channels, *Int. J. Rem. Sens.*, **22**, 1269-1283.

Weatherhead, E. C., G. C. Reinsel, G. C. Tiao, X.-L. Meng, D. Choi, W.-K. Cheang, T. Keller, J. DeLuisi, D. J. Wuebbles, J. B. Kerr, A. J. Miller, S. J. Oltmans, and J. E. Frederick, 1998: Factors affecting the detection of trends: Statistical considerations and applications to environmental data, *J. Geophys. Res.*, **103**, 17,149-17,161.

Weatherhead, E. C., G. C. Reinsel, G. C. Tiao, C. H. Jackman, L. Bishop, S. M. Hollandsworth Frith, J. DeLuisi, T. Keller, S. J. Oltmans, E. L. Fleming, D. J. Wuebbles, J. B. Kerr, A. J. Miller, J. Herman, R. McPeters, R. M. Nagatani, and J. E. Frederick, 2000: Detecting the recovery of total column ozone, *J. Geophys. Res*., **105**, 22,201-22,210.

Wielicki, B. A., B. R. Barkstrom, E. F. Harrison, R. B. Lee III, G. L. Smith, and J. E. Cooper (1996), Clouds and the Earth's Radiant Energy System (CERES): An Earth observing system experiment, *Bull. Amer. Meteor. Soc., 77*, 853-868.

Wielicki, B. A., T. Wong, R. P. Allan, A. Slingo, J. T. Kiehl, B. J. Soden, C. T. Gordon, A. J. Miller, S. –K. Yang, D. A. Randall, F. Robertson, J. Susskind, H. Jacobowitz, 2002: Evidence for large decadal variability in the tropical mean radiative energy budget, *Science*, **295**, 841-844.

Wielicki, B. A., T. Wong, N. Loeb, P. Minnins, K. Priestley, and R. Kandel, 2005: Changes in Earth's albedo measured by satellite, *Science*, **308**, 825.

Wolter, K., and M.S. Timlin, 1993: Monitoring ENSO in COADS with a seasonally adjusted principal component index. *Proc. of the 17th Climate Diagnostics Workshop*, Norman, OK, NOAA/N MC/CAC, NSSL, Oklahoma Clim. Survey, CIMMS and the School of Meteor., Univ. of Oklahoma, 52-57.

Wolter, K., and M.S. Timlin, 1998: Measuring the strength of ENSO - how does 1997/98 rank? *Weather*, **53**, 315-324.

Wong, T., B. A. Wielicki, R. B. Lee, III, G. L. Smith, and K. A. Bush, 2006: Re-examination of the observed decadal variability of Earth radiation budget using altitude-corrected ERBE/ERBS Nonscanner WFOV data, *J. Climate* (in press).

Zhang, Y.-C., W. B. Rossow, and A. A. Lacis, 1995: Calculation of surface and top of atmosphere radiative fluxes from physical quantities based on ISCCP data sets: 1. Method and sensitivity to input data uncertainties, *J. Geophys. Res*., **100**, 1149–1165.

Zhang, Y., W. B. Rossow, A. A. Lacis, V. Oinas, and M. I. Mishchenko (2004), Calculation of radiative fluxes from the surface to top of atmosphere based on ISCCP and other global data sets: Refinements of the radiative transfer model and the input data, *J. Geophys. Res*., **109**, D19105, doi:10.1029/2003JD004457.

Figures

Figure 1 Daily 30°N-30° S oceanic average CERES SW radiances against MODIS (a) 0.65 mm and (b) 0.86 mm radiance for May 2000. Lines correspond to regression fits to the data.

Figure 2 The year-to-year relative calibration stability of CERES and MODIS determined by comparing predicted mean radiances from regression relations in each year with predicted mean radiances from regression relations derived in 2000 (see Eq. (2)).

Figure 3 Scatterplot of footprint-average MISR and MODIS (a) red and (b) near-infrared radiances for all CERES footprints over ocean between 30°S and 30°N on September 12, 2000. One-to-one line is indicated.

Figure 4 Same as Fig. 2 but for MISR and MODIS.

Figure 5 (a) Deseasonalized monthly anomalies in SeaWiFS PAR (Einstein m^{-2} day^{-1}) and CERES Terra FM1 SW TOA flux (Wm^{-2}) over ocean for 30°S-30°N from March 2000–June 2005; (b) Same as Fig. 5a except that SeaWiFS PAR anomalies are scaled by a factor of -6.58, corresponding to the slope of the regression line fit relating CERES SW TOA flux and SeaWiFS PAR anomalies. The solid and dotted lines without symbols in Fig. 5b correspond to regression line fits to the SeaWiFS and CERES anomalies, respectively.

Figure 6 Slope of the SeaWiFS PAR—CERES SW Flux anomaly regression line for the tropical ocean regions listed in Table 4.

Figure 7 (a) Deseasonalized monthly anomaly in CERES SW TOA flux for land and multivariate ENSO index for 30°S-30°N; (b) scatterplot of CERES monthly SW TOA flux anomaly and multivariate ENSO index.

Figure 8 (a) Deseasonalized monthly anomalies in CERES Terra FM1 and CERES Aqua FM4 all-sky SW TOA flux (Wm-2) for (a) 30°S-30°N and (b) 90S-90N from August 2002–March

2005. The solid and dotted lines without symbols correspond to regression line fits to the anomalies.

Figure 9 (a) Deseasonalized monthly anomalies in CERES Terra FM1 and ISCCP FD RadFlux all-sky SW TOA flux (Wm-2) for (a) 30°S-30°N and (b) 90°S-90°N from August 2002–March 2005. The solid and dotted lines without symbols correspond to regression line fits to the anomalies.

Figure 10 Number of years to detect a given trend in SW TOA flux anomaly with 50% and 90% probability for (a) 30°S-30°N and (b) 90°S-90°N.

Tables

Source	Parameter(s)	Product/Version	Temporal Coverage
CERES *Terra* (FM1)	SW Unfiltered Radiance SW TOA Flux	SSF Ed2B_rev1	03/2000 – 06/2005
MODIS *Terra*	Nadir Radiance in 0.64 μm and 0.86 μm Bands Cloud Fraction Aerosol Optical Depth	SSF Ed2B_rev1 (Collection 4)	03/2000 – 06/2005
MISR *Terra*	Nadir Radiance in 672 nm and 867 nm Bands	SSFM Ed2B (Collections 5 and 6)	Selected September Days (2000 – 2004)
CERES *Aqua* (FM4)	SW TOA Flux	SSF Ed2A_rev1	08/2002 – 03/2005
SeaWiFS SeaStar	Photosynthetically Active Radiation	Version 5.1	03/2000 – 06/2005
ISCCP	SW TOA Flux	FD RadFlux (Zhang et al., 2004)	03/2000 – 12/2004

Table 1 List of datasets considered in this study.

Time Period/Region	Variable	σ (Wm^{-2})	σ(D) (Wm^{-2})	r^2
03/2000-06/2005 30°S-30°N (Ocean)	SeaWiFS PAR	0.76	0.21	0.93
	CERES *Terra* SW TOA Flux	0.79		
03/2000-06/2005 30°S-30°N	CERES *Terra* SW TOA Flux	0.83	-	-
03/2000-06/2005 30°S-30°N (Land)	CERES *Terra* SW TOA Flux	0.32	-	-
03/2000-06/2005 90°S-90°N	CERES *Terra* SW TOA Flux	0.55	-	-
08/2002-03/2005 30°S-30°N	CERES *Aqua* SW TOA Flux	0.77	0.42	0.75
	CERES *Terra* SW TOA Flux	0.81		
08/2002-03/2005 90°S-90°N	CERES *Aqua* SW TOA Flux	0.44	0.36	0.48
	CERES *Terra* SW TOA Flux	0.48		
03/2000-12/2004 30°S-30°N	ISCCP SW TOA Flux	1.2	0.91	0.43
	CERES *Terra* SW TOA Flux	0.85		
03/2000-12/2004 90°S-90°N	ISCCP SW TOA Flux	1.1	0.97	0.19
	CERES *Terra* SW TOA Flux	0.56		

Table 2 Summary of monthly anomaly statistics for each data record comparison; σ=standard deviation in monthly anomalies; σ(D)=standard deviation of the difference between monthly anomalies from two data records.

Time Period/Region	Variable	Slope (Wm^{-2} per decade)	95% Conf. Invl. in Slope (Wm^{-2} per decade)	Slope of Anomaly Difference (Wm^{-2} per decade)
03/2000-06/2005 30°S-30°N (Ocean)	SeaWiFS PAR	0.41	(-0.8, 1.6)	-0.02±0.3
	CERES *Terra* SW TOA Flux	0.43	(-0.9, 2.0)	
03/2000-06/2005 30°S-30°N	CERES *Terra* SW TOA Flux	-0.26	(-1.6, 1.1)	-
03/2000-06/2005 30°S-30°N (Land)	CERES *Terra* SW TOA Flux	-0.69	(-1.2, -0.2)	-
03/2000-06/2005 90°S-90°N	CERES *Terra* SW TOA Flux	-0.59	(-1.5, 0.3)	-
08/2002-03/2005 30°S-30°N	CERES *Aqua* SW TOA Flux	-3.5	(-6.9, -0.073)	-3.5±1.5
	CERES *Terra* SW TOA Flux	0.031	(-3.8, 3.9)	
08/2002-03/2005 90°S-90°N	CERES *Aqua* SW TOA Flux	-2.9	(-4.7, -1.1)	3.8±1.0
	CERES *Terra* SW TOA Flux	0.93	(-1.3, 3.2)	
03/2000-12/2004 30°S-30°N	ISCCP SW TOA Flux	0.75	(-1.5, 3.0)	1.4±1.7
	CERES *Terra* SW TOA Flux	-0.64	(-2.3, 1.0)	
03/2000-12/2004 90°S-90°N	ISCCP SW TOA Flux	1.8	(-0.2, 3.8)	2.5±1.7
	CERES *Terra* SW TOA Flux	-0.76	(-1.8, 0.3)	

Table 3 Summary of monthly anomaly trends and uncertainties.

Region	Latitude/Longitude Range	Slope of Anomaly Difference (Wm^{-2} per decade)
Southwest Tropical Ocean	30°S-0°S 180°W-0°W	-4.5 ± 1.5
Southeast Tropical Ocean	30°S-0°S 0°E-180°E	-0.076 ± 1.5
Northwest Tropical Ocean	0°N-30°N 180°W-0°W	2.8 ± 1.1
Northeast Tropical Ocean	0°N-30°N 0°E-180°E	2.1 ± 2.4

Table 4 Slope of SeaWiFS and CERES anomaly difference (SeaWiFS minus CERES) by region.

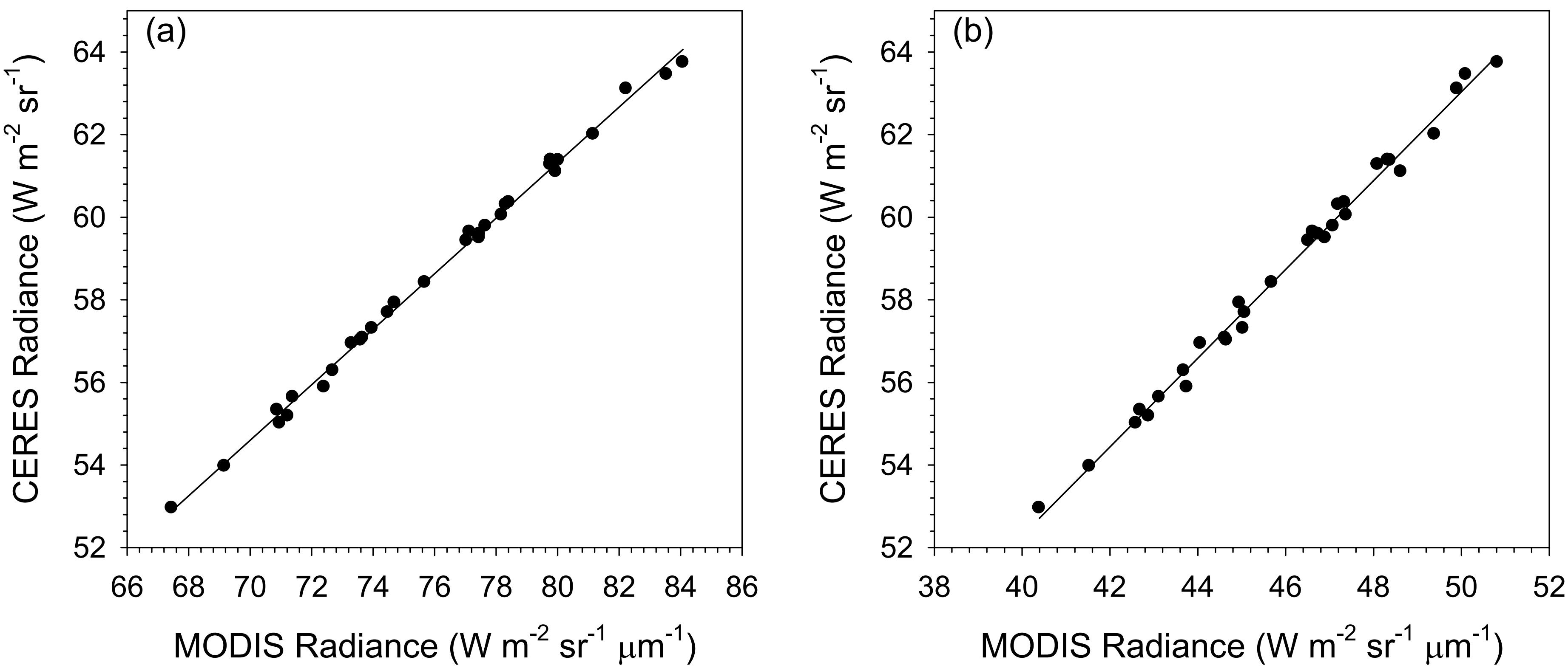

Figure 1 Daily average CERES SW radiances against MODIS (a) 0.65 μm and (b) 0.86 μm radiance for May 2000. Lines correspond to regression fits to the data.

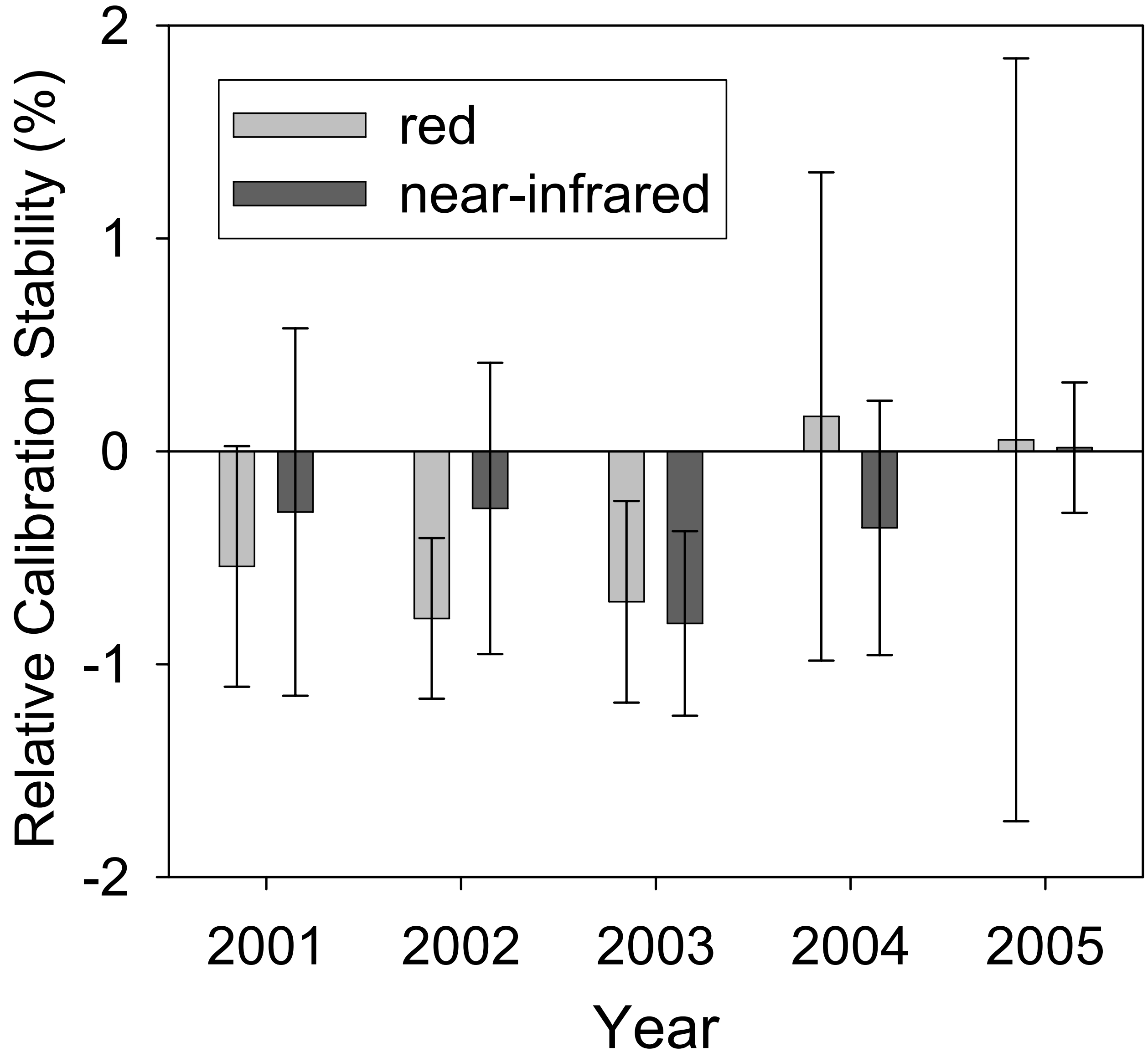

Figure 2 The year-to-year relative calibration stability of CERES and MODIS determined by comparing predicted mean radiances from regression relations in each year with predicted mean radiances from regression relations derived in 2000 (see Eq. (2)). Error bars correspond to 95% confidence intervals in the relative calibration stability.

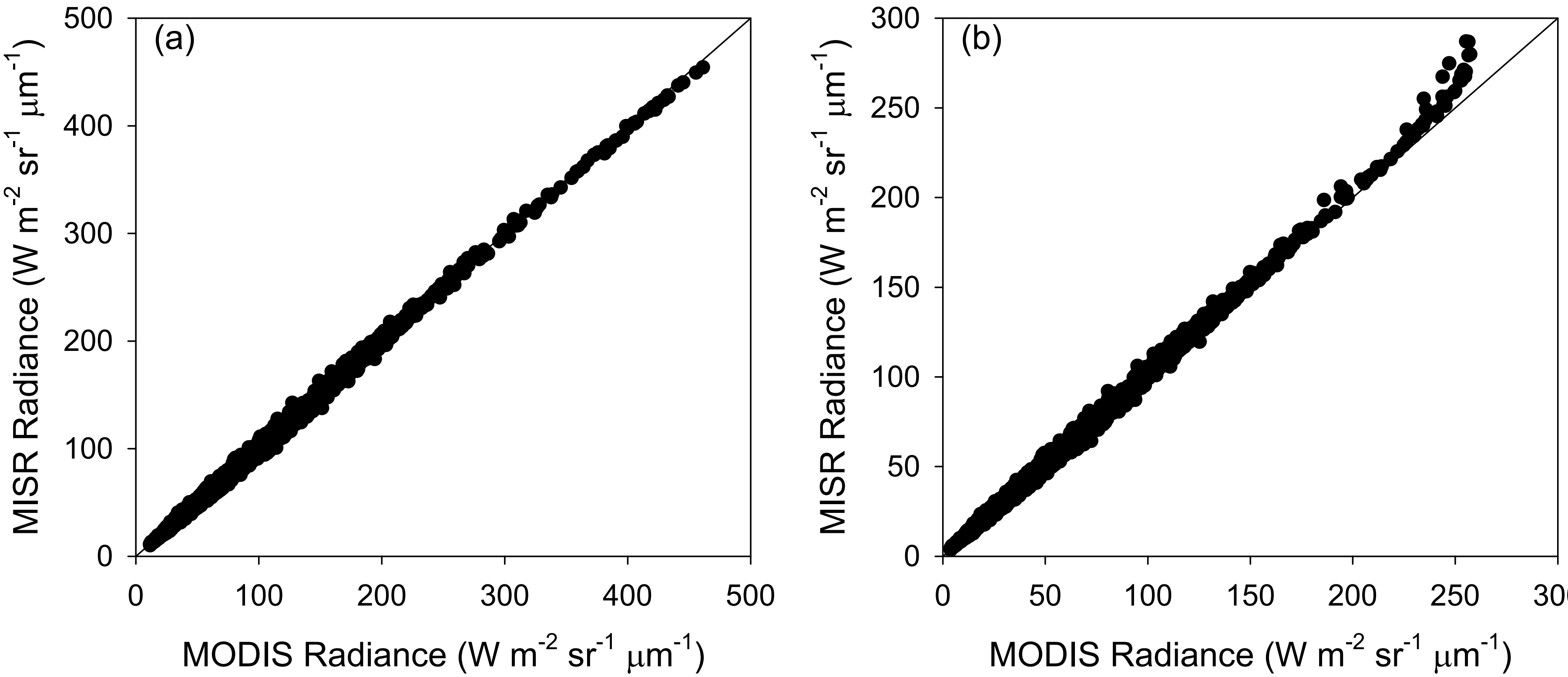

Figure 3 Scatterplot of footprint-average MISR and MODIS (a) red and (b) near-infrared radiances for all CERES footprints over ocean between 30°S and 30°N on September 12, 2000. One-to-one line is indicated.

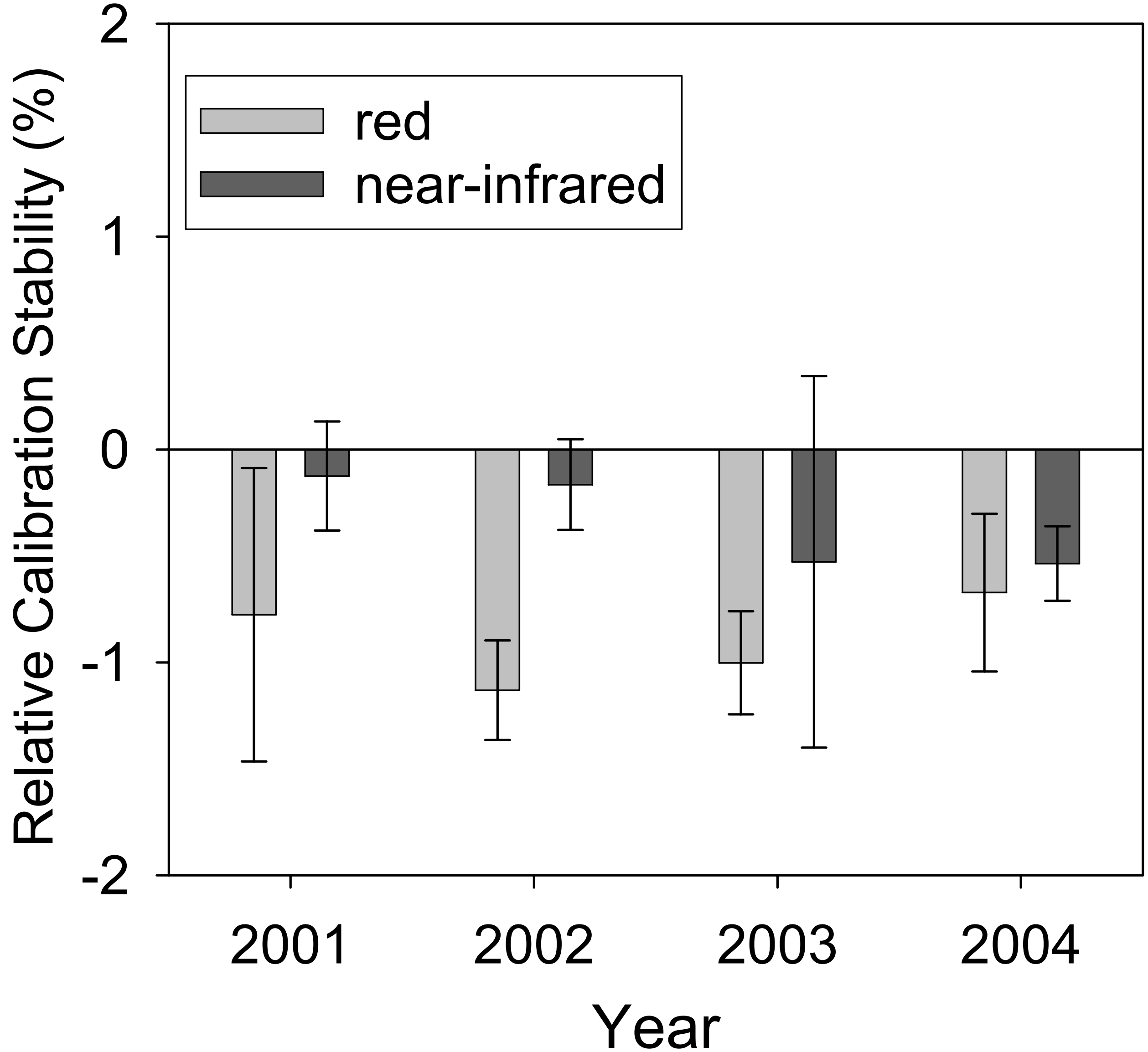

Figure 4 Same as Fig. 2 but for MISR and MODIS.

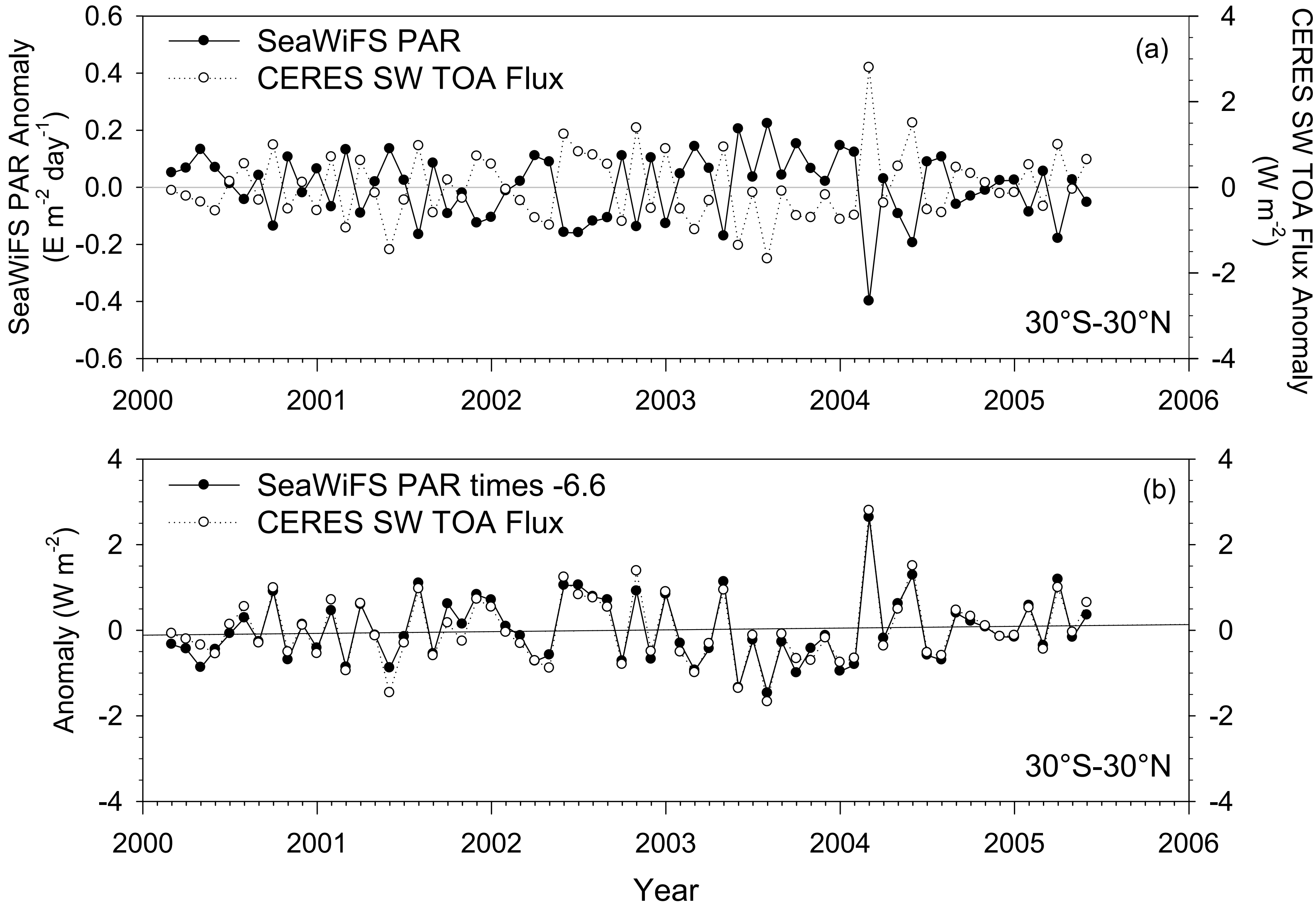

Figure 5 (a) Deseasonalized monthly anomalies in SeaWiFS PAR (E m^{-2} day^{-1}) and CERES *Terra* FM1 SW TOA flux (W m^{-2}) over ocean for 30°S-30°N from March 2000–June 2005; (b) Same as Fig. 5a except that SeaWiFS PAR anomalies are scaled by a factor of -6.58, corresponding to the slope of the regression line fit relating CERES SW TOA flux and SeaWiFS PAR anomalies. The solid and dotted lines without symbols in Fig. 5b correspond to regression line fits to the SeaWiFS and CERES anomalies, respectively.

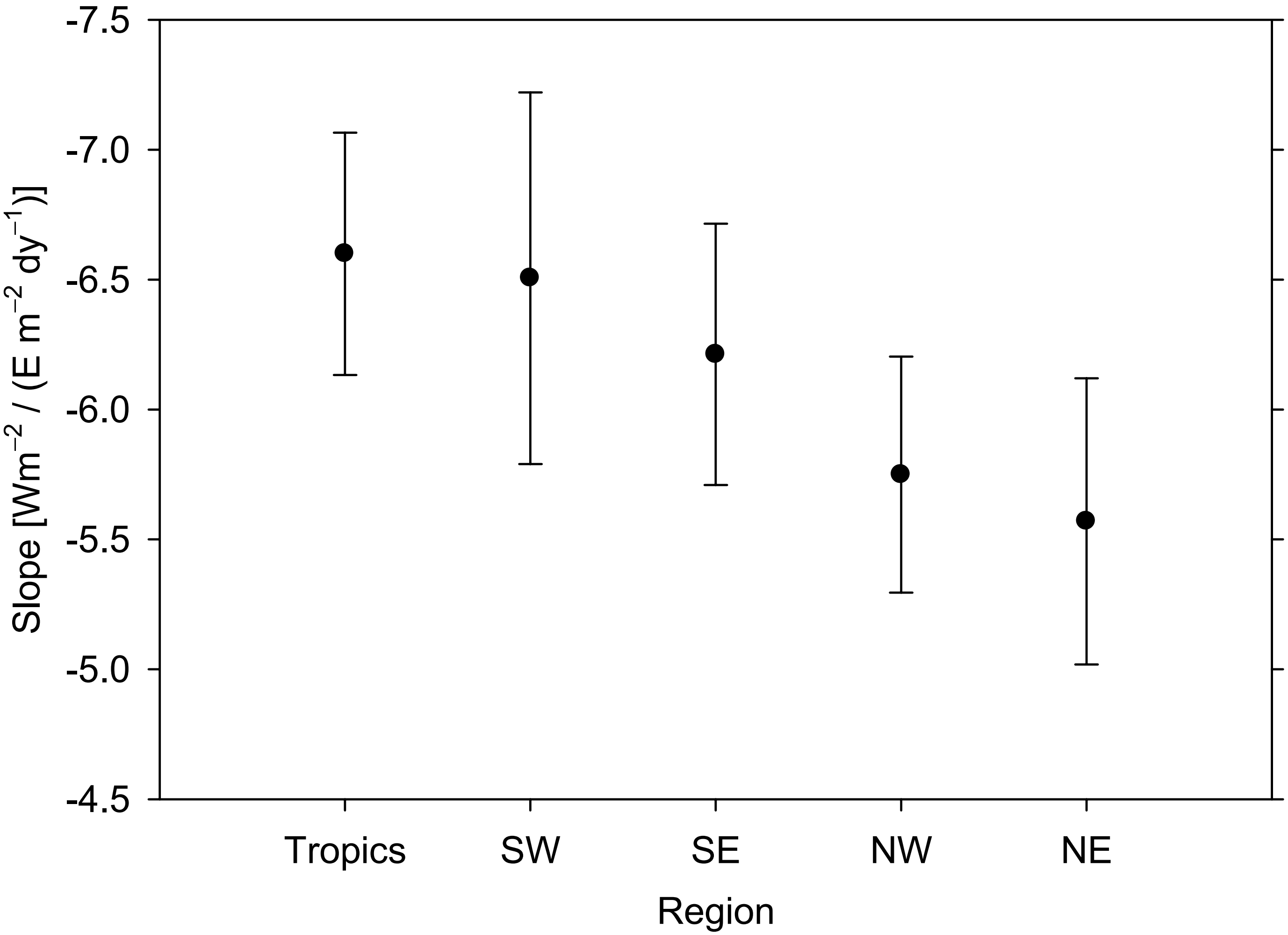

Figure 6 Slope of the SeaWiFS PAR—CERES SW Flux anomaly regression line for the tropical ocean regions listed in Table 4.

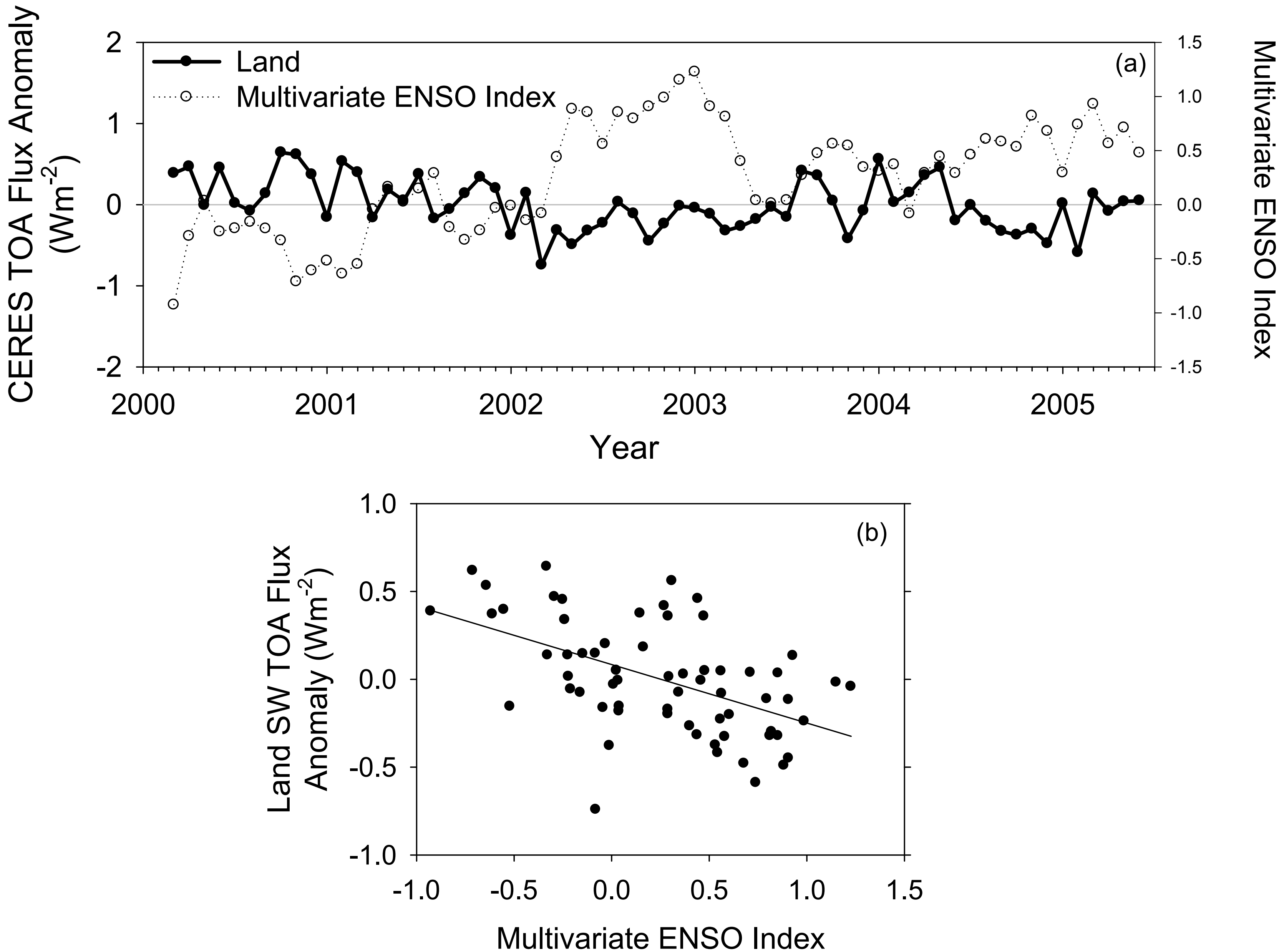

Figure 7 (a) Deseasonalized monthly anomaly in CERES SW TOA flux for land and multivariate ENSO index for 30°S-30°N; (b) scatterplot of CERES monthly SW TOA flux anomaly and multivariate ENSO index.

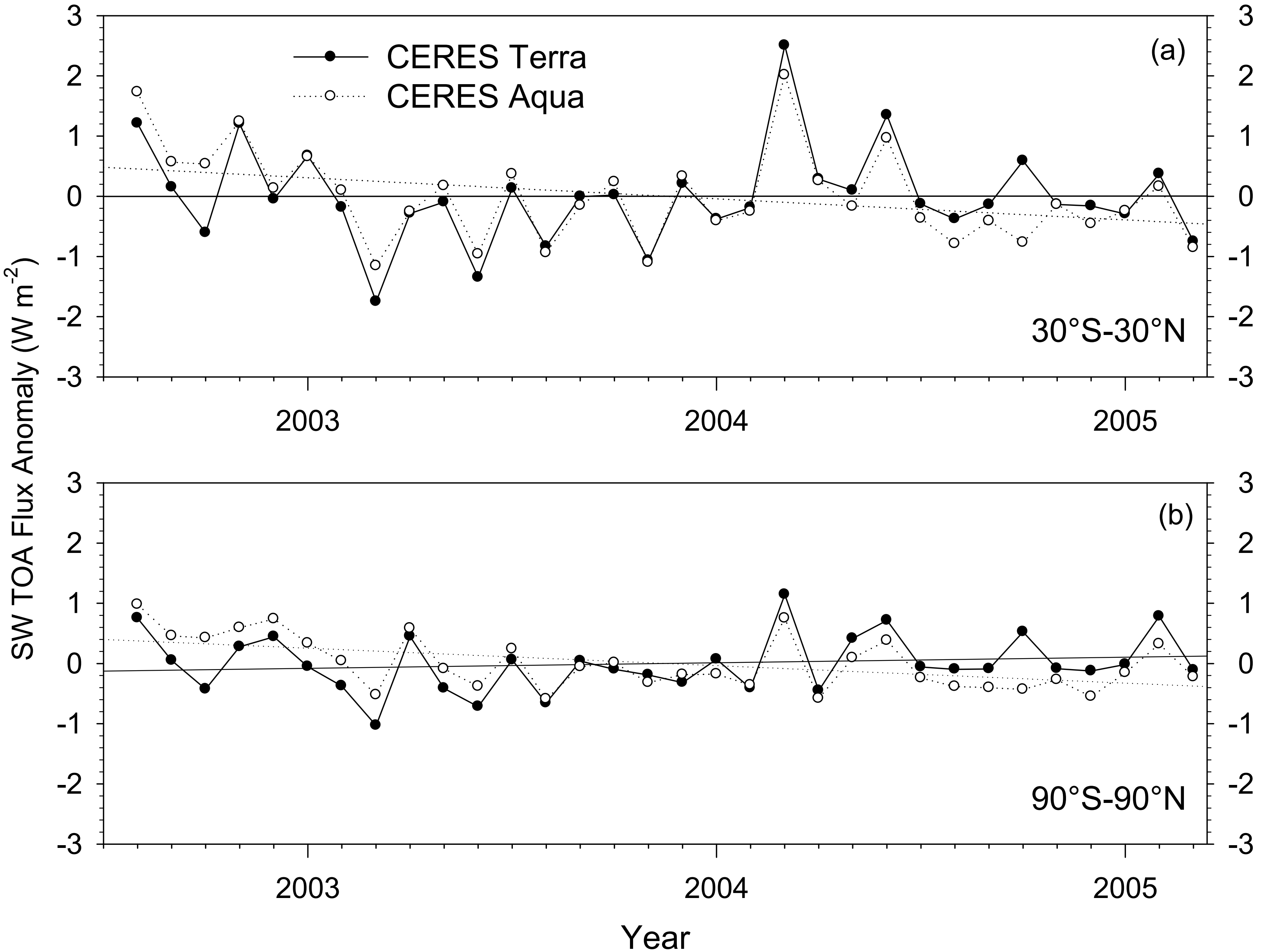

Figure 8 (a) Deseasonalized monthly anomalies in CERES *Terra* FM1 and CERES *Aqua* FM4 all-sky SW TOA flux (W m^{-2}) for (a) 30°S-30°N and (b) 90°S-90°N from August 2002–March 2005. The solid and dotted lines without symbols correspond to regression line fits to the anomalies.

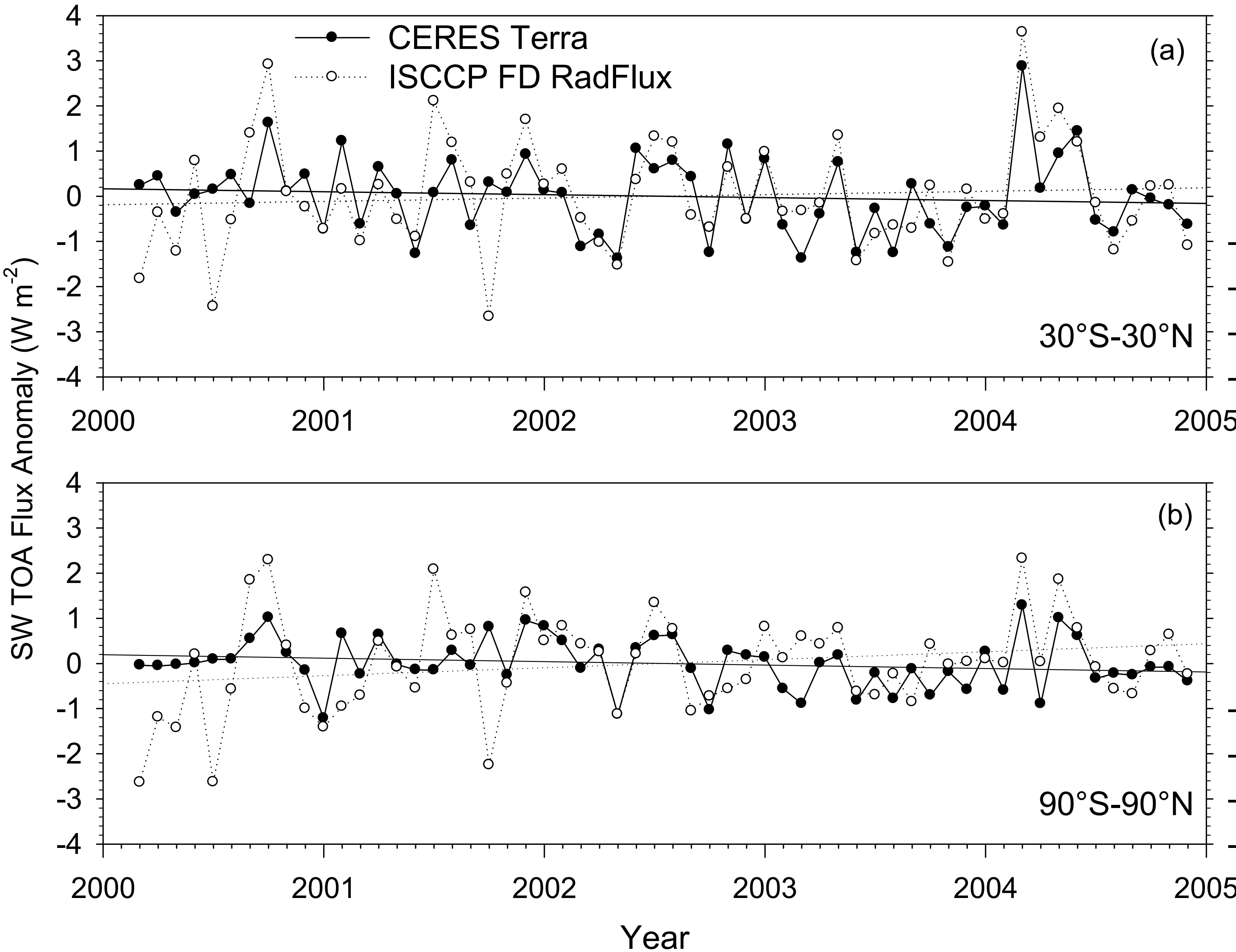

Figure 9 (a) Deseasonalized monthly anomalies in CERES *Terra* FM1 and ISCCP FD RadFlux all-sky SW TOA flux (W m^{-2}) for (a) 30°S-30°N and (b) 90°S-90°N from August 2002–March 2005. The solid and dotted lines without symbols correspond to regression line fits to the anomalies.

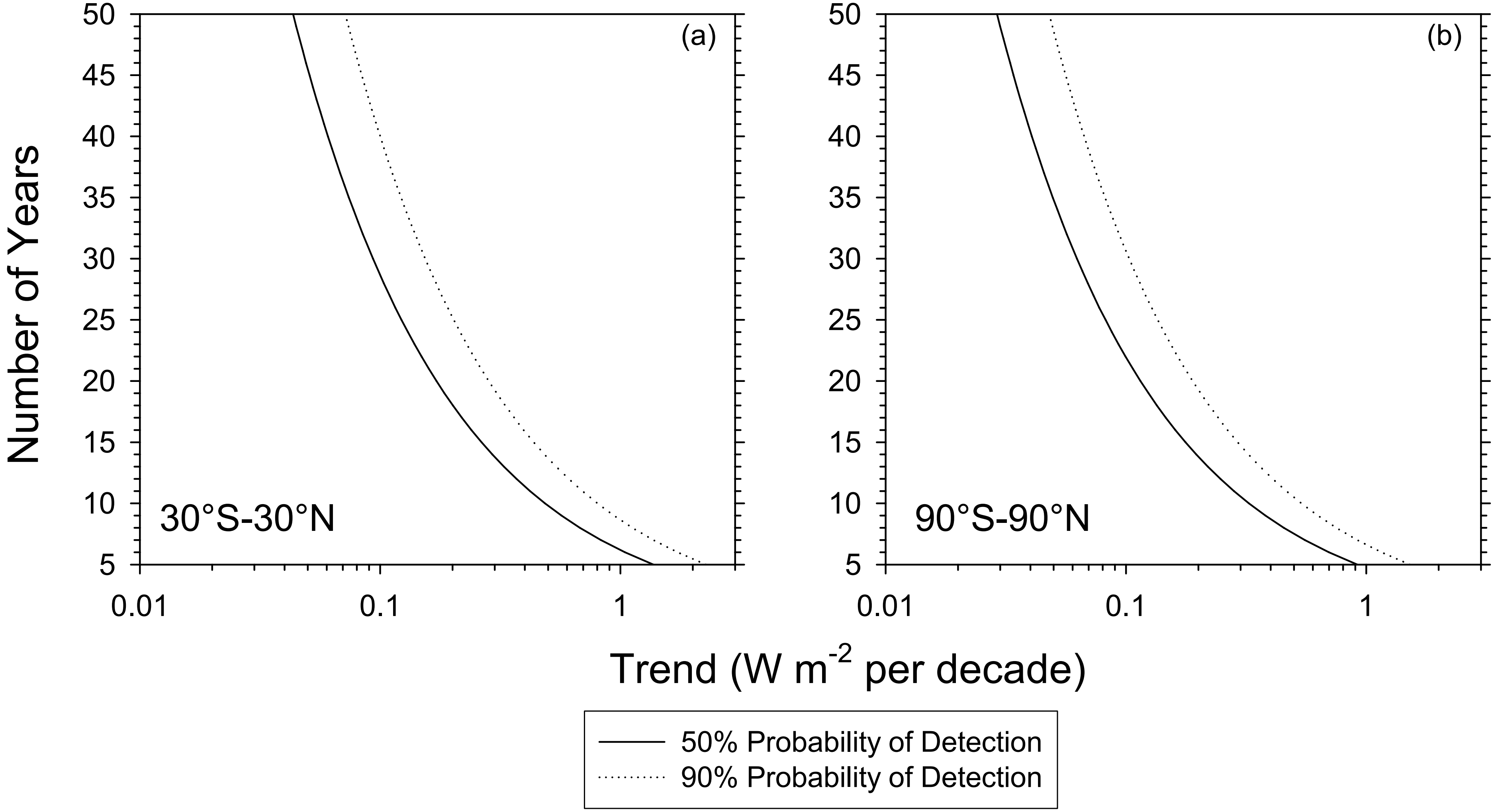

Figure 10 Number of years to detect a given trend in SW TOA flux anomaly with 50% and 90% probability for (a) 30°S-30°N and (b) 90°S-90°N.